https://ntrs.nasa.gov/search.jsp?R=19930083604 2020-06-17T20:39:30+00:00Z

Y 3. N21/5:6/2845

GOVT. DOC.
BUSINESS AND TECHNICAL DEPT. Jan 9 '53

NATIONAL ADVISORY COMMITTEE FOR AERONAUTICS

TECHNICAL NOTE 2845

X-RAY INSTRUMENTATION FOR DENSITY MEASUREMENTS IN A SUPERSONIC FLOW FIELD

By John Dimeff, Ralph K. Hallett, Jr., and
C. Frederick Hansen

Ames Aeronautical Laboratory
Moffett Field, Calif.

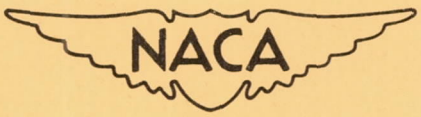

Washington
December 1952

NATIONAL ADVISORY COMMITTEE FOR AERONAUTICS

TECHNICAL NOTE 2845

X-RAY INSTRUMENTATION FOR DENSITY MEASUREMENTS IN A SUPERSONIC FLOW FIELD

By John Dimeff, Ralph K. Hallett, Jr., and
C. Frederick Hansen

SUMMARY

An X-ray beam is essentially undeviated while traversing a short path in air. At wave lengths of approximately 6 Angstroms, sufficient absorption occurs in air to allow satisfactory measurement of densities at a total density as low as approximately 2×10^{-5} g per cubic centimeter. An instrument based on this principle is described. The advantages of this type of instrument accrue from the fact that, refractive effects being negligible, data are related to path elements geometrically fixed with respect to the tunnel.

In its present form the X-ray densitometer was used to measure the product of the air density and the path length in the Ames 10- by 14-inch supersonic wind tunnel. The instrument gave data for the average density-path-length of a 0.025-centimeter-diameter cylindrical section of the air stream, normal to the direction of air flow.

The measurement is accomplished by comparing the intensity of two beams from the same X-ray source. Both beams have the same path length and pass through the same number of windows. Thus, the only difference in the two paths is that due to the absorption within the wind tunnel.

INTRODUCTION

The present necessity for more detailed study of such phenomena as occur in high-velocity aerodynamic shock waves and boundary layers around wind-tunnel models has forced an increasing effort to obtain accurate quantitative data of localized flow fields. The techniques most generally pursued to obtain local densities have been those related to optical interferometry. While the fundamental accuracy and the basic simplicity of such optical methods are great, results are inaccurate since the change in the measured quantity is a function of both the magnitude of the change being measured and the geometrical position at which the

change occurs. These methods are limited further because present techniques do not allow for the production and maintenance of optical elements of sufficient accuracy to meet the requirements of very high-speed low-density flow. As a result of these limitations, increased effort has been made to find a method not subject to the prodigious obstacles to analysis or to the limitations regarding usable density range.

A technique introduced by Arnold (reference 1) makes use of the absorption of a narrow beam of soft X rays normal to the direction of air flow. The method makes use of the intensity of an X-ray beam as measured by an ionization chamber as an indication of the integrated gas density across the test section. The particular advantage accruing from this approach results from the fact that in the X-ray region, the index of refraction of most gases is sufficiently near unity that refractive effects can be neglected without error.

Winkler (reference 2) revised the experimental techniques of Arnold to include the use of a Geiger-Mueller type X-ray detector, and simultaneous intensity monitoring. With the revised technique Winkler was able to use a beam cross-section area of 1.3×10^{-2} square centimeters and to obtain a maximum error of 1.2×10^{-4} grams per square centimeter in the measurement of integrated density-path-length.

Weltmann, Fairweather, and Papke (reference 3) were able to obtain accuracies of the same order of magnitude with similar equipment using a beam area of 3×10^{-3} cm^2. By using a beam of narrow rectangular cross section the latter experimenters were able to increase the resolving power in one direction to about 25 times that obtained by Winkler (reference 2). The notable advance achieved by the equipment described in reference 3, however, was the reduction of total X-ray-beam area required for the accuracies described. This decrease in beam area required an increase of the time needed to record a single measurement point by a factor of ten.

The equipment described in this report achieves a greater accuracy than those described in references 2 and 3 while utilizing a smaller beam cross section and a shorter recording time. This equipment was developed specifically for use in the Ames 10- by 14-inch supersonic wind tunnel which operates at densities as low as 2×10^{-5} g/cm^3.

SYMBOLS

A area of sphere whose radius is equal to the anode to detector spacing, square centimeters

c ratio of λ_2 to λ_1

E anode potential of the X-ray tube, volts

I intensity of beam after absorption, quanta per second

I_o intensity of beam before absorption, quanta per second

l tunnel width, centimeters

N number of electrons per second delivered to the anode of the X-ray tube

n number of quanta required per second from X-ray tube

P area of X-ray detection device window, square centimeters

U ratio of the number of quanta produced to the number of impinging electrons

x length of absorbing medium, centimeters

z atomic number of absorbing medium

z_a atomic number of X-ray-tube anode material

λ wave length of X radiation, Angstroms

μ linear absorption coefficient, centimeters^{-1}

$\frac{\mu}{\rho}$ mass absorption coefficient, square centimeters per gram

ρ density of absorbing medium, grams per cubic centimeter

ρ_s density of disturbed stream, grams per cubic centimeter

ρ_{so} density of free stream, grams per cubic centimeter

ANALYSIS OF SYSTEM REQUIREMENTS

The absorption of energy from an X-ray beam by a homogeneous material produces an exponential decrease in the intensity of the beam in accordance with Lambert's law

$$I = I_o \epsilon^{-\mu x} \tag{1}$$

which may be rewritten

$$ln \frac{I}{I_o} = - \mu x$$

where

I_o initial intensity of the X-ray beam

I intensity after absorption

x length of the absorbing medium

μ linear absorption coefficient, the product of the density, ρ, and the mass absorption coefficient, μ/ρ, for the frequency of the X radiation and the absorbing material used

It is apparent from the above equation that, for conditions wherein the frequency of the X radiation, the path length, and the nature of the absorbing material are known, the density of the absorbing material can be related directly to the natural logarithm of the ratio of intensity of the X-ray beam after absorption in the test medium to the intensity of an unabsorbed reference beam (see fig. 1). This affords a basic approach to the problem around which instrumentation can be designed. There are a number of factors which affect the intensity of the initial beam, such as the condition of the X-ray-tube target, variations of filament current and plate current, etc. The technique of simultaneously measuring the two intensities and of indicating the ratio between a test beam and a reference beam originating from the same source allows a closer approach to the ultimate sensitivity of the system by providing a partial cancellation of such effects.

The absorption in air varies for different wave lengths of X rays, the longer wave lengths being more readily absorbed. The absorption coefficient for X rays, within limited wave-length ranges, can be expressed by (reference 4)

$$\frac{\mu}{\rho} = k\lambda^3 z^4 \qquad (2)$$

where

$\frac{\mu}{\rho}$ mass absorption coefficient for the absorbing medium

λ wave length of the radiation

z atomic number of the absorbing material

k a constant within a limited wave-length region

By inserting the value of μ obtained from the above into equation (1) we obtain, for wave lengths λ_1 and λ_2,

$$\left.\begin{aligned} I_{\lambda_1} &= I_{O\lambda_1}\epsilon^{-(k\lambda_1^3 z^4 x\rho)} \\ I_{\lambda_2} &= I_{O\lambda_2}\epsilon^{-(k\lambda_2^3 z^4 x\rho)} \end{aligned}\right\} \tag{3}$$

If

$$I_{O\lambda_1} = I_{O\lambda_2}$$

then

$$\frac{I_{\lambda_1}}{I_{\lambda_2}} = \epsilon^{(x\mu_{\lambda_1})(c^3-1)} \tag{4}$$

where

$$\lambda_2 = c\lambda_1$$

It is seen from equation (4) that a selective absorption process occurs in which the logarithm of the intensity ratio for two wave lengths is proportional to the absorption $\mu_{\lambda_1} x$ and in which the intensity of the longer wave-length radiation is rapidly reduced. If a continuous X-radiation spectrum is used as a source, this selective absorption process tends to shift the effective radiation toward a shorter, more penetrating wave length. In order to obtain an instrument sensitive to low air densities, it is necessary to arrange the physical construction of the instrument in such a manner that a minimum of the sensitive long wave-length radiation is absorbed in windows, etc., outside the test section. This condition can be favored by using a single window of low absorption material separating the X-ray tube and the test volume instead of separate windows with an intervening air space.

For high accuracy and sensitivity the primary sensing device must be stable and highly efficient. Detectors for X rays are based on several effects: photoelectric effects, photographic effects, ionization effects, etc. Of the many possible detectors available the Geiger-Mueller tube was chosen as the most suitable since, by proper design, relatively high efficiency, temperature stability, etc., can be assured. An objectionable characteristic of this detector is the statistical error associated with the finite inactive time following each count. Since the production and absorption of quanta are of a random nature, the existence of such an inactive period means that a fractional number of the total

quanta will not be detected by the G-M tube. A statistical error is thus introduced whose magnitude depends upon the length of the inactive period and the mean interval between quanta.

The ratio technique previously described allows partial cancellation of statistical errors since the errors occur simultaneously in both the measuring tube and the reference tube. The normal device used to detect G-M tube impulses will respond to impulses greater than a certain minimum magnitude. This minimum value of impulse magnitude occurs after a minimum time interval composed of the G-M tube "dead" time and the portion of its recovery time necessary to allow the impulse from the succeeding quantum to reach the minimum value required by the detecting circuit. Since both these intervals depend on the anode voltage of the G-M tube, this voltage must be regulated in order to prevent variations in the statistical error. Even with the anode voltages on the two G-M tubes regulated, the difference in indications of different pairs of tubes with the reference and measuring chambers evacuated have been found to cause an indicated ratio of as much as from 0.8 to 1.2. This initial variation is to be expected from the G-M tube differences and from slight differences in geometry; that is, effects of target angle, window thickness, etc. The resulting variation of initial ratio does not introduce error in the use of the instrument as long as this ratio is known and remains constant during the tests.

It will be assumed, for the present, that indicating equipment can be designed to meter the intensity of an X-ray beam accurately within 1 percent exclusive of statistical errors. It will also be considered possible to produce an X-ray source for which the ratio of quanta produced within two fixed solid angles is stable within 1 percent. Since the limit of usability of an instrument is approached when the signal-to-noise (or error) ratio approaches unity in value, the change in the intensity of the X-ray beam after traversing the tunnel should be at least 2 percent for a tunnel density change of approximately 10^{-6} g/cc (corresponding to 5 percent of the lowest density to be attained).

From equation (1) we obtain the ratio of intensities of two beams having equal initial intensity and having traversed an absorption path of the same length and different densities

$$\frac{I_2}{I_1} = \epsilon^{x(\mu_1-\mu_2)}$$

$$= \epsilon^{x(\mu/\rho)(\rho_1-\rho_2)}$$

from which

$$\frac{\mu}{\rho} = \frac{\ln(I_2/I_1)}{x(\rho_1-\rho_2)} \tag{5}$$

where

$\rho_1-\rho_2$ density difference

μ linear absorption coefficient

$\frac{\mu}{\rho}$ mass absorption coefficient of the test medium

I_1, I_2 intensities of the beams after absorption

x distance traversed

The minimum free-stream density to be attained by the tunnel is 5×10^{-5} g/cc. If the instrument is characterized by a 2-percent error and must measure a density change of 10^{-6} g/cc over a path length of 25 cm, the mass absorption coefficient required is then

$$\frac{\mu}{\rho} = \frac{\ln(1.02)}{25(10^{-6})}$$

$$\approx 790$$

This value of mass absorption coefficient corresponds closely to that of nitrogen and oxygen in the region of 6 Angstroms.

Generation of X rays in the region of 6 Angstroms is most easily accomplished by using the continuous radiation spectrum. The shortest wave-length radiation λ_o produced by an anode excited by electrons of a voltage E is given (reference 4) by

$$\lambda = \frac{1.2(10^4)}{E} \tag{6}$$

The efficiency of production of X rays is given (reference 4) by

$$U = 1.1\ (10^{-9})\ z_a E \tag{7}$$

where

U ratio of number of quanta produced to number of impinging electrons

z_a atomic number of the anode material

If the detection equipment can be made to respond satisfactorily to a quantum rate of n quanta per second, the total number of electrons per second which must be delivered to the anode is given (reference 4) by

$$N = \frac{An}{PU} \tag{8}$$

where

N number of electrons per second

n number of quanta required per second

A area of sphere whose radius equals anode to detector spacing

P area of the detection device

We obtain from equations 6, 7, and 8

$$N = 0.76 \frac{An\lambda}{Pz_a} \times 10^5$$

Assuming an anode to detector distance of 37.5 cm, a tungsten anode, a receiver radius of 0.025 cm, a required counting rate of 1,000 counts per second and a wave length of 6 Angstroms,

$$N = 5.55 \times 10^5 \quad \text{electrons per second}$$

or

$$N = 8.9 \times 10^{-5} \quad \text{amperes}$$

Since this is the current required when the X-ray beam is not diminished in intensity, the anode current available in the X-ray high-voltage power supply should exceed this value by some large factor depending on the nature and number of windows and the absorption range to be covered.

The intensity variation is proportional to anode current variation, and from equation 6 it is seen that the shortest wave length produced is inversely proportional to the voltage which accelerates the electrons. Since the minimum wave length produced and, therefore, the effective mass absorption coefficient vary with the accelerating voltage, it is essential that the voltage be maintained constant in order to hold constant calibration.

The assumptions previously made regarding the stability of production and the stability of intensity measurements of X rays have been proved practicable in actual laboratory tests. It was found that the desired results could be achieved satisfactorily by using conventional

electronic regulators for the G-M tube anode supply, and for the X-ray tube anode and filament supplies (regulation approximately 0.25 percent). The regulated power supply controls filament current to maintain constant anode current. The desired accuracy of indication can be achieved readily by utilizing the ratio technique in conjunction with the detector circuits described in the following sections.

EQUIPMENT

The physical arrangement of the X-ray source, quanta detectors, and reference chamber with respect to the test section of the Ames 10- by 14-inch supersonic wind tunnel is shown schematically in figure 1. The X-ray tube shown in the figure has two anodes to permit simultaneous measurements at two separate positions. The equipment for the production and ratio metering of the X-ray-beam energy meets the salient requirements established in the previous section: the X-ray anode and the detecting element (Geiger-Mueller tubes) can each be separated from the test chamber by a single window; and the intensity of the X-ray beam can be monitered by the reference G-M tube so that the density of the test medium may be related directly to the intensity ratio.

Figure 2 is a photograph of the partially disassembled X-ray tube. Figure 3 shows details of the focusing anode and cathode structures. The focusing structure mounted on the cathode of the X-ray tube allows the use of an electron source which is large in area and focuses the electron beam within an area of a few square millimeters on the anode. This reduces the instabilities and errors which can occur as a result of thermal shifting of the cathode, migration of the effective anode spot, and differences in the target efficiency at different surface elements. The filament used was a five-turn helical coil with a diameter of 0.3 cm and a length of 0.6 cm and was of 0.032-cm-diameter thoriated tungsten wire. Water cooling was provided to reduce anode gassing effects and to reduce possible errors due to changes in production efficiency with anode temperature.

Figure 4 presents data on absorption losses in a few of the window materials tested. It is apparent that cellophane is the most suitable window material at anode voltages above 1.8 kilovolts. Since it was found that after long usage the cellophane windows had a tendency to rupture, the X-ray tube has been designed for a constantly evacuated system to facilitate replacement of windows and cathodes.

The G-M tube used in the final installation is shown in figure 5. It is an argon filled tube with an organic quenching admixture. It possesses the following nominal characteristics:

1. Counting efficiency, 99 percent
2. Window, 0.003-cm cellophane, 0.5-cm diameter
3. Plateau length, two hundred volts
4. Plateau slope, 3 percent per hundred volts
5. Maximum background count, 40 per minute
6. Maximum dead time, 50 microseconds

Regulation of the X-ray-tube anode potential and current is required to prevent changes in production efficiency, intensity, and wave length which would result from fluctuations in anode voltage and anode current. The regulated power supplies were obtained on special contract from a commercial concern. They are capable of supplying anode currents of from 0 to 50 milliamperes each to as many as four anodes, and have performance characteristics commensurate with the requirements established in the analysis above.

Diagrams showing interconnections and interlocking between the main power supply and the electronic control and indicating circuits are given in figures 6 and 7. In order to permit duplication of components of the system, schematic wiring diagrams of the components are given in detail in figures 8 through 12. A list of components for these circuits is given in table I. Component designations which are not preceded by a letter are terminal points. The first number of each component designation identifies the particular component associated with the electronic circuit. Interconnections can be followed by reference to the interconnection diagram (fig. 6). Necessary interlocking and control circuits are included in a control unit for which the schematic diagram is shown in figure 7.

Voltage is supplied to the G-M tubes from a commercial regulated voltage supply and a distribution panel (fig. 8). Operation of the G-M tubes is indicated visually by a gas tube scaling circuit and neon indicator bulbs. The quenching circuit (fig. 9) used in conjunction with the G-M tube derives its power from the high-voltage distribution panel and power supply (fig. 8). A low-impedance tube (V301) is used in this quenching circuit to discharge the G-M anode. The control elements of this tube are directly coupled to the plates of a single-shot multivibrator which is triggered by the beginning of the G-M tube discharge.

The impulses derived from the quenching circuits for the G-M tube monitoring the intensity of the reference beam and the G-M tube monitoring the intensity of the test beam are fed into two shaping and indicating circuits. Each circuit (fig. 10) consists of a conventional pulse amplifier and a triggered single-shot multivibrator. The output pulse of the multivibrator is clipped and applied to a condenser and twin diode circuit which transfers a small amount of charge to a storage condenser. This charge, then, is independent of the shape or amplitude of input pulse. The diode, which transfers the charge to the storage condenser,

is biased in such a manner that contact potentials will not affect output readings. Circuit elements in this charging circuit are chosen so that the total voltage developed on the storage condenser, for designed pulse-repetition rates, remains small compared to the voltage amplitude of the clipped pulse. The charge transferred to the storage condenser in this circuit is accurately proportional to the repetition rate of the input triggering impulse. By adjusting the pulse widths of the two multivibrators the ratio meters are adjusted to give equal charge transfer to the output circuits for the reference and the measuring storage condensers. With the same number of pulses per second injected into both sides, the charge leakage rates from the two storage condensers are made equal by varying the leakage resistance across one condenser until the voltage developed on that condenser equals the voltage developed on the other storage circuit. Calibration linearity is checked by varying the ratio of the input trigger pulses and comparing the output voltage from the storage condenser on the reference side with the output voltage from the measuring side. The difference between these two voltages is fed into a "chopper" amplifier (fig. 11) which is used to energize a phase-sensitive motor. This motor drives a voltage divider on the output of the reference rate meter in such a manner as to reduce the difference between the two signals. when this difference is zero, the position of the linear voltage divider is an indication of the ratio of the average recurrence rates of the pulses being fed into the two circuits; and, therefore, of the ratio of intensities of the two X-ray beams. This ratio meter is provided with a counter-type indicator connected to, and indicating the position of, the voltage divider driven by the chopper amplifier.

The complete ratio metering installation as described above is checked by means of a test and calibration curcuit (fig. 12). Simulated G-M tube pulses are generated by two separate multivibrators and pulse-shaping circuits. The frequency of one multivibrator is adjusted to approximately 1,000 pulses per second. The second multivibrator is synchronized to the first multivibrator and switched to frequencies related to the control frequency by factors of 1.00, 0.75, 0.50, and 0.25. Figure 13 shows the indicated frequency ratio taken from the counter as a function of the ratio of the repetition rates of the impressed test signal. Data are given for the same ratios at several different impulse frequencies.

The vacuum equipment used in conjunction with the X-ray tube is of conventional design. An oil diffusion pump backed by a mechanical pump is used. A Pirani gage and an ionization gage are used to indicate pressure in the X-ray tube. These gages are interlocked with the electrical controls for the system (fig. 7) in order to insure that operation of the X-ray tube does not occur without sufficient vacuum and in order to simplify operation of the over-all equipment.

CALIBRATIONS AND TESTS

Laboratory Calibration

The laboratory calibration was accomplished with the equipment mounted on a test chamber in which the air density could be varied. The anode potentials of the G-M tubes were adjusted so that the tubes were operated within their plateau regions. With the anode voltage of the X-ray tube adjusted to the desired value as determined by the desired degree of sensitivity of the X-ray beam, the anode current was adjusted to provide an X-ray-beam intensity that would give approximately 1,000 pulses per second from the reference G-M tube. The indicated ratio of intensities of the reference beam and test beam was recorded for the condition wherein the densities in the reference and test chambers were both zero (less than 10^{-7} g/cc). In subsequent operations the G-M tube anode voltages were adjusted, when necessary, to provide this same indicated ratio with both chambers at zero density. This procedure eliminated variations in calibration resulting from the effect of differing voltages on dead time and recovery time of the G-M tubes. The reference chamber was maintained at zero density throughout the calibration and use of the equipment in the laboratory.

The calibration was accomplished by adjusting the density of the air in the path of the measuring beam to known values. The values of this density and the indicated values of intensity ratio for the two X-ray beams were recorded and form an over-all system calibration for the particular value of X-ray anode voltage used. A complete calibration was obtained by repeating the above procedure for several values of anode voltage.

Typical laboratory calibration data are presented in figures 14 and 15. Figure 14 shows over-all instrument sensitivities for X-ray-tube anode voltages of 2.0 and 1.7 kv. For these data the maximum deviation from a straight line is of the order of 10^{-5} g/cm^2. Figure 15 presents data taken at an X-ray-tube anode voltage of 2.0 kv for two separate tests. The data presented in figures 14 and 15 were obtained with an X-ray-beam area of 8×10^{-3} cm^2 and with an electrical integrating time of 5 minutes. The data of figure 15 indicate a repeatability of density-path-length calibration of the order of 10^{-5} g/cm^2.

Wind-Tunnel Calibration

The final calibration was accomplished in the Ames 10- by 14-inch supersonic wind tunnel. The arrangement of the X-ray source, quanta detectors, etc., was as shown in figure 1 except that only one beam was used. For calibration, a cylindrical tube was placed between the walls so that the density within could be changed at will. This arrangement

made it possible for the calibration to include any geometrical factors introduced by the tunnel mounting. Two circular apertures (one at each wall) of approximately 0.025 cm diameter (5×10^{-4}-cm^2 area) were used to define the X-ray beam through the test section of the tunnel. This reduced aperture as compared with the laboratory tests was necessary to increase the spatial resolution of the instrument. The areas of the apertures defining the X-ray beam through the reference chamber were adjusted so that the ratio of the outputs from the G-M tubes was unity when the densities were zero in both beam paths. During wind-tunnel calibration the averaging time was reduced from 5 minutes to 30 seconds.

As the density to be measured increases, the ratio between the intensities of the test and reference beams may exceed the range of the ratio-metering equipment (i.e., between 0.20 and 1.20). This requires adjustment of the reference beam to bring the ratio into range. Since the reference-beam apertures were fixed once the initial alinement was made, subsequent adjustments of output ratio for the tunnel calibrations were made by regulating the density in the reference chamber. The selective absorption of the air shifts the effective intensity-distribution spectrum of the beam to shorter wave lengths as the reference and measured air densities are increased. Thus the effective mass-absorption coefficient decreases with increasing density-path-length, making it necessary to calibrate the densitometer for each reference density-path-length as well as for each X-ray-tube anode voltage used. With the density in the reference chamber and the anode voltage fixed, the ratio of G-M tube outputs was measured as a function of the density-path-length in the test beam.

From the beginning of the calibration runs until the completion of the tunnel tests, no changes in equipment settings were made except the resetting of X-ray-tube conditions to the voltages and currents desired for particular run conditions and the replacement of a G-M detector tube found to be acting erratically. The sensitivity of the instrument was found to be stable and relatively independent of G-M tubes. The limits of accuracy established for tunnel operation include such variations as were caused by the faulty G-M tube just prior to its replacement and by such differences as may have existed between the replacement tube and that used during earlier calibration.

Typical calibration data are shown in figure 16. The logarithm of the output ratio is very nearly a linear function of density-path-length traversed by the test beam. The least-squares lines fitting the measured data were calculated and the slopes of these lines are the calibration constants of the densitometer used to convert output ratios to density-path-lengths. The standard error of the calibration data with respect to the least-squares line is less than 5×10^{-5} g/cm^2 in each case. This sensitivity is consistent with the 10^{-5} g/cm^2 found in the laboratory calibration when allowance is made for the smaller beam area and the decreased averaging time used in the wind tunnel, since the square of the

statistical error is approximately inversely proportional to the number of counts received (i.e., to the product of the aperture area and the averaging time interval used).

The calibration constants for several operating voltages and reference density-path-lengths are listed in table II.

The logarithm of the intensity ratio is theoretically a linear function of density-path-length for a monochromatic beam of X rays (equation 5). The X-ray beams used are admittedly not monochromatic; nevertheless, the results are linear within the limits of experimental accuracy. The calibration constants in table II are the effective mass absorption coefficients for the beam of mixed wave lengths for the particular path lengths and reference density concerned.

Wind-Tunnel Tests

At the conclusion of this calibration in the wind tunnel the chamber was removed from between the tunnel side walls and a 40°-cone model was placed in position so that the X-ray beam was contained in a plane perpendicular to the cone axis 7.32 cm downstream of the apex.

The flow field about the model was scanned by moving the model with respect to the beam. This movement was accomplished by rotating the model on a double bent sting which offset the model axis 1.90 cm parallel to the axis of rotation of the sting (fig. 17).

The densitometer measures the average density across the entire wind tunnel, including the boundary layers, so the measured value of density-path-length when the model flow field is clear of the beam path is used as a reference. The differences between measured density-path-lengths and this reference value result from perturbations of the stream due to the model.

Measurements were taken at Mach numbers from 3.49 to 4.98. In figure 18, the measured perturbations in density-path-length through the flow field of the 40° cone are compared with the values according to the Taylor-Maccoll conical flow theory. The theoretical ratios of the densities in the conical flow to the free-stream density ρ_s/ρ_{so} were obtained for the Mach numbers of the test by graphical interpolation of the values calculated from the Taylor-Maccoll theory by Kopal (reference 5). Stream-density perturbation fractions $(\rho_s-\rho_{so})/\rho_{so}$ were plotted as functions of position in the flow and these curves were graphically integrated along the path of the beam. The integrals were multiplied by the corresponding free-stream densities in the Ames 10- by 14-inch supersonic

wind tunnel[1] to yield the theoretical perturbations in the density-path-length along the X-ray beams.

Since the Taylor-Maccoll theory is exact for inviscid flow and has been well verified experimentally, the deviations of the experimental data from the theory are taken as a measure of the accuracy of the X-ray densitometer under actual test conditions. These deviations were generally within the standard error of the calibration measurements (5×10^{-5} g/cm^2). The deviations relative to the total density-path-length across the wind tunnel increase with decreasing stream density (i.e., increasing Mach number), so the maximum relative deviations vary from about 1 percent at Mach number 3.49 (total density-path-length 78.4×10^{-4} g/cm^2) to 5 percent at Mach number 4.98 (total density-path-length 6.95×10^{-4} g/cm^2).

For two-dimensional flow, the incremental density values would be obtained simply by dividing the path-length factor out of the measured values of the incremental density-path-length product. For three-dimensional flow the mean incremental density is the difference between integrands of the equation,

$$\Delta\rho_s l = \int_0^l \rho_s dx - \int_0^l \rho_{so} dx \tag{9}$$

This equation can be solved in the case of axially symmetric flow by iteration methods developed for the reduction of interferometer fringe-shift data (reference 7). However, it is inherent in these methods that the errors are cumulative unless they are random. As a consequence of this cumulative error, the density increments in the conical flows corresponding to the data presented in figure 18 have mean deviations from the Taylor-Maccoll theory which vary from 1 percent at Mach number 3.49 to as much as 12 percent at the highest Mach numbers tested.

---

[1]With the normal reservoir conditions (6 atmospheres total pressure and 295° K total temperature) the free-stream density in the wind tunnel is related to the reservoir density through the usual isentropic flow equations at the test Mach numbers 3.49 and 4.03. However, at Mach numbers of 4.48 and greater the air stream is partially condensed and the stream Mach number and density were determined using the method presented by Hansen and Nothwang (reference 6). The effects of the condensation account for the low theorical values of density-path-length encountered at Mach numbers 4.48, 4.67, 4.84, and 4.98.

CONCLUDING REMARKS

The X-ray densitometer described in this report determined density-path-length perturbations of low-density supersonic flow in the Ames 10- by 14-inch supersonic wind tunnel within better than $\pm 5 \times 10^{-5}$ g/cm^2 using a beam area of 5×10^{-4} cm^2 and a point recording time of approximately 30 seconds. This sensitivity and resolution should be adequate for the investigation of thin flow regions such as boundary layers and shock waves. With G-M detectors of improved stability and uniformity and with increased reading time interval per datum point, the laboratory accuracy of 1×10^{-5} g/cm^2 should be more nearly approached.

The X-ray density measuring equipment, wherein a beam technique is employed, suffers from two fundamental objections: First, a long tunnel running time is required as a result of the necessity for a point-to-point survey; second, a rapid qualitative survey of the flow field is not practicable. However, the method is not subject to refraction errors such as occur in the interferometer technique.

The methods and instrumentation described are not intended to represent the ultimate capabilities of the X-ray technique. With development of lower absorption windows and more efficient electron sources, the sensitivity of the present beam technique can further be improved.

Ames Aeronautical Laboratory
National Advisory Committee for Aeronautics
Moffett Field, California

REFERENCES

1. Arnold, G.: Dichtemessungen mit Röntgenstrahlen an Uberschallstromungen im Windkannal. Peenemünde Heeresversuchsstelle, (Aerodynamisches Institut), Archiv 66/124, Jan. 11, 1944.

2. Winkler, Eva: Density Measurements by Means of the X-Ray Absorption Method. NOL Memo 10,118, 1949.

3. Weltman, Ruth N., Fairweather, Steven, and Papke, Daryl: Application of X-Ray Absorption to Measurement of Small Air-Density Gradients. NACA TN 2406, 1951.

4. Compton, Arthur H., and Allison, Samuel K.: X-Rays in Theory and Experiment. D. Van Nostrand Co., Inc., N. Y., 1935.

5. Mass. Inst. of Tech., Dept. of Elec. Engr., Center of Analysis. Tables of Supersonic Flow Around Cones. By the Staff of the Computing Section, Center of Analysis, under the direction of Zdenek Kopal. Tech. Rep. No. 1, Cambridge, 1947.

6. Hansen, C. Frederick, and Nothwang, George J.: Condensation of Air in Supersonic Wind Tunnels and Its Effects on Flow About Models. NACA TN 2690, 1952.

7. Weyl, F. Joachim: Analytical Methods in Optical Examination of Supersonic Flow. Navy Dept., Bur. Ord., NAVORD Rep. 211-45, Dec. 1945.

TABLE I.- CIRCUIT COMPONENTS

Battery

B102-3 volt

Condensers

C101-.0005
C102-.001
C103-.1
C104-8
C105-.005
C106-200 mmfd
C107-3 mmfd
C108-.05
C109-.002
C110-.25
C111-8
C112A,B-16
C113A,B-16
C114-.01
C115-.01
C201-500
C202-500
C301-40 mmfd 2000V
C302-100 mmfd 600 V
C303-100 mmfd
C304-.001
C501-.001
C502-.001
C503-06-10 mmfd
C507-.001
C508-10 mmfd
C509-10 mmfd
C510-200 mmfd
C511-400 mmfd
C512-.001
C513-.001
C514-17-.01
C518-25-.003
C526-10 mmfd
C701-8
C702-8
C703-.005
C704-40 mmfd
C705-.01
C706-.01
C707-.002

Pilot Lights

I901-6-8V Pilot Lamp
I902-6-8V Pilot Lamp
I903-6-8V Pilot Lamp
I904-6-8V Pilot Lamp

Relays

K901-120V AC relay 3 PDT
K902-120V AC relay 3 PDT
K905-120V AC relay 3 PDT
K907-120V AC relay 3 PDT
K908-120V AC relay 3 PDT
K909-120V AC relay 3 PDT
K920-120V AC relay 3 PDT
K951-120V AC relay 3 PDT
K959-120V AC relay 3 PDT
K952-2000 ohm 1 ma DC DPDT

TABLE I.- CONTINUED

Resistors

R101-10K
R102-100
R103-30K
R104-4.9K
R105-2.7K
R106-30K
R107-.27M
R108-.12M
R109-30K
R110-5K
R112-50K
R113-.1M
R114-30K
R115-18K
R116-2.5K ± 1%
R117-30K
R118-1.5K
R120-500 ± .1%
R121-100 pot.
R122-10K
R123-500 pot.
R124-100 ± .1%
R125-10K pot.
R201-3.3K
R202-3.3K
R203-10K) ganged ten
R204-10K) turn pot.
R301-.1M
R302-20K
R303-3.3K
R304-26K
R305-.1M
R306-.1M
R307-.1M
R308-2.2K
R501-150K
R502-150K
R503-.25M
R504-.5M
R505-.5M
R506-10K
R507-.1M
R509-.15M
R510-.1M pot.
R511-10K
R512-.1M
R513-.1M
R514-.15M
R515-.15M
R516-.5M
R517-10K
R518-.1M
R519-.1M
R520-.1M
R521-10K
R522-.5M
R523-.15M
R524-.1M
R525-.25M
R526-.5M
R527-.5M
R528-.5M
R529-.5M
R530-33-.1M
R701-48-70K
R749-56-.5M
R758-35K
R759-33K
R760-67K
R761-.1M
R762-.1M
R763-.1M
R764-67K
R765-67K
R766-.1M
R767-10M
R768-.1M
R769-4.7K
R770-40K
R771-2M
R772-4.7K
R773-(5)20M

TABLE I.- CONCLUDED

Switches

S901-push button N.O.
S902-push button N.C.
S903-push button N.O.
S904-push button N.C.

Transformers

T101-800V C.T. 200 ma
T701-700V C.T. 90 ma
T702-6.3V C.T.
T703-6.3V C.T.
T901-6.3V

Vacuum Tubes

V101-03-6SN7
V104-6H6
V105-5U4G
V301-2C26A
V302-12AT7
V501-5692
V502-6SN7
V503-5692
V504-6SN7
V505-08-5651
V701-5Y4
V702-03-2050
V704-12AU7

Rectifier

Y901-115V 50 ma dry rectifier

NOTE

K = 1,000 ohms
M = 1,000,000 ohms
mmfd = micro-microfarad
All capacitance values are in microfarads except where noted.
All resistance values are ohms except where noted.

TABLE II.- X-RAY DENSITOMETER CALIBRATION CONSTANTS

X-ray-tube anode voltage	Reference density-path-length	Calibration constant
2.25 kv	0 g/cm^2	-645 cm^2/g
2.62 kv	0	-530
2.75 kv	14.0×10^{-4}	-449
3.00 kv	27.0×10^{-4}	-368
3.25 kv	46.0×10^{-4}	-242
3.62 kv	72.0×10^{-4}	-154

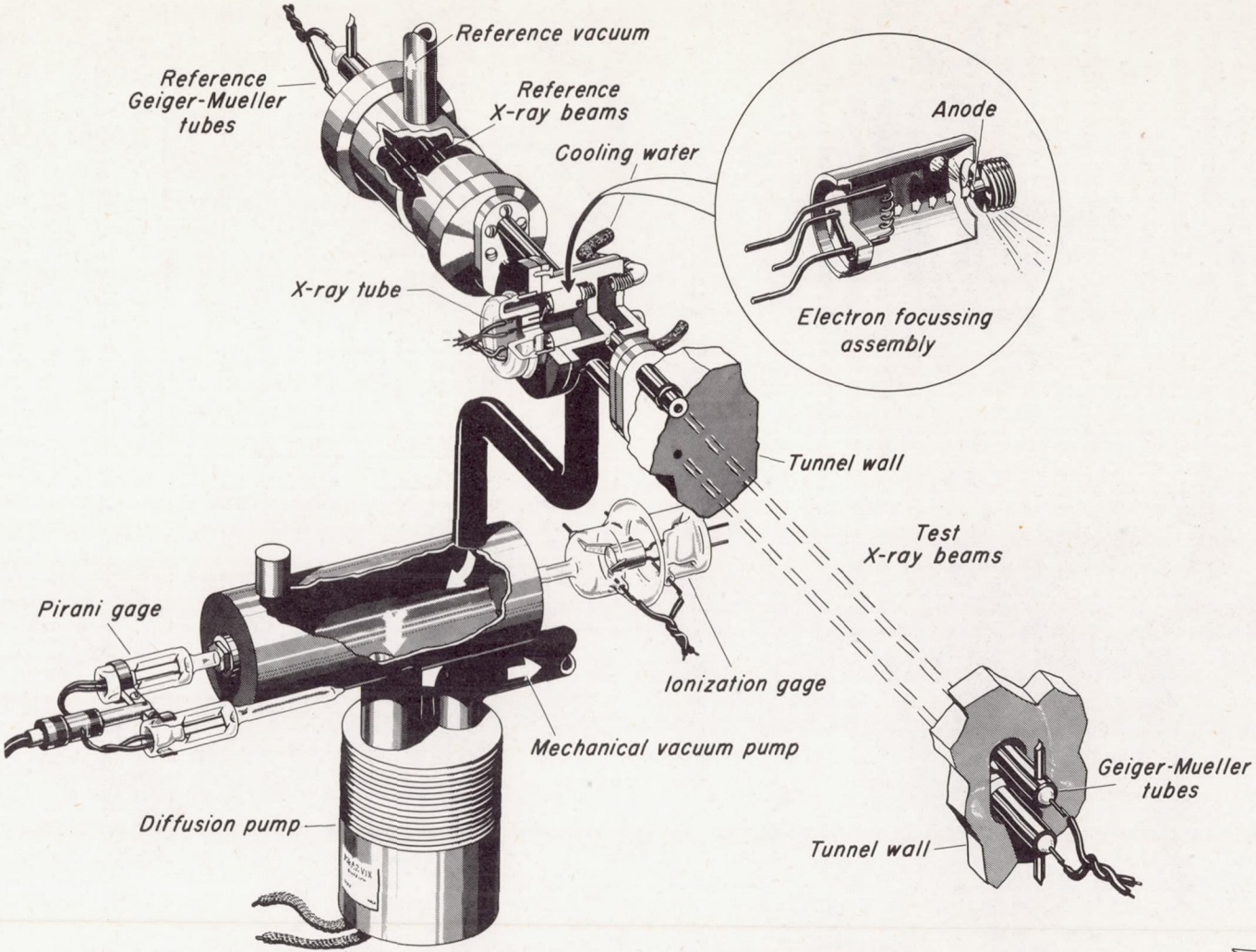

Figure 1.- Physical arrangement of the X-ray source and detectors relative to the test section of the 10- by 14-inch Supersonic Wind Tunnel.

NACA
A-17460

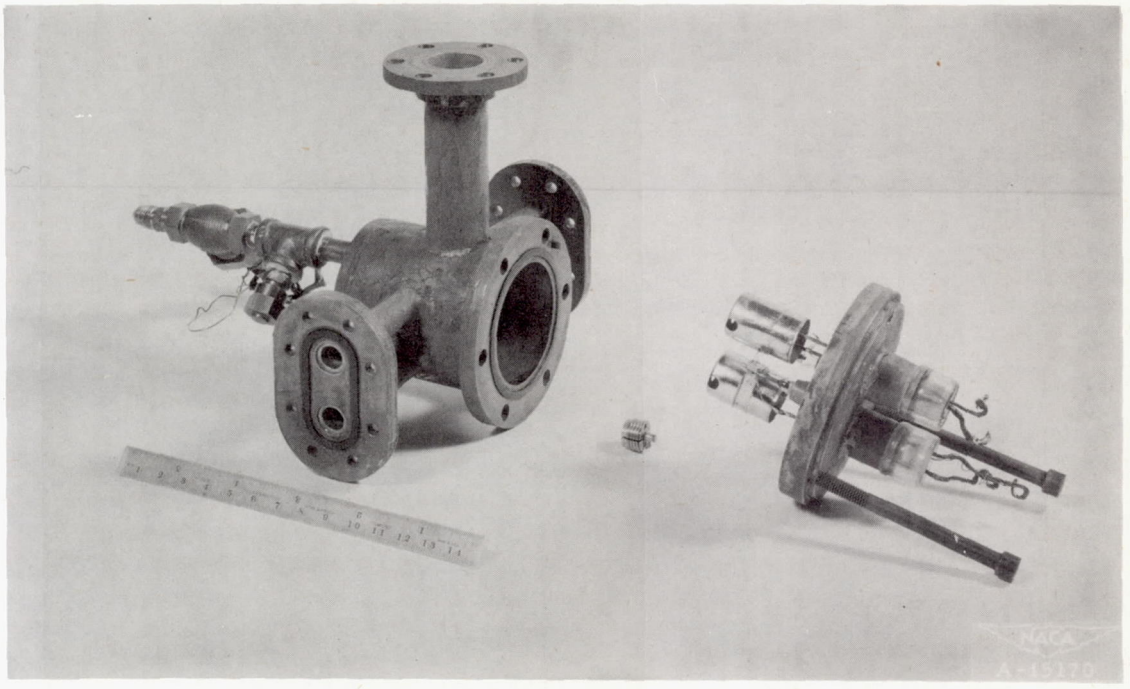

Figure 2.- Photograph of X-ray tube.

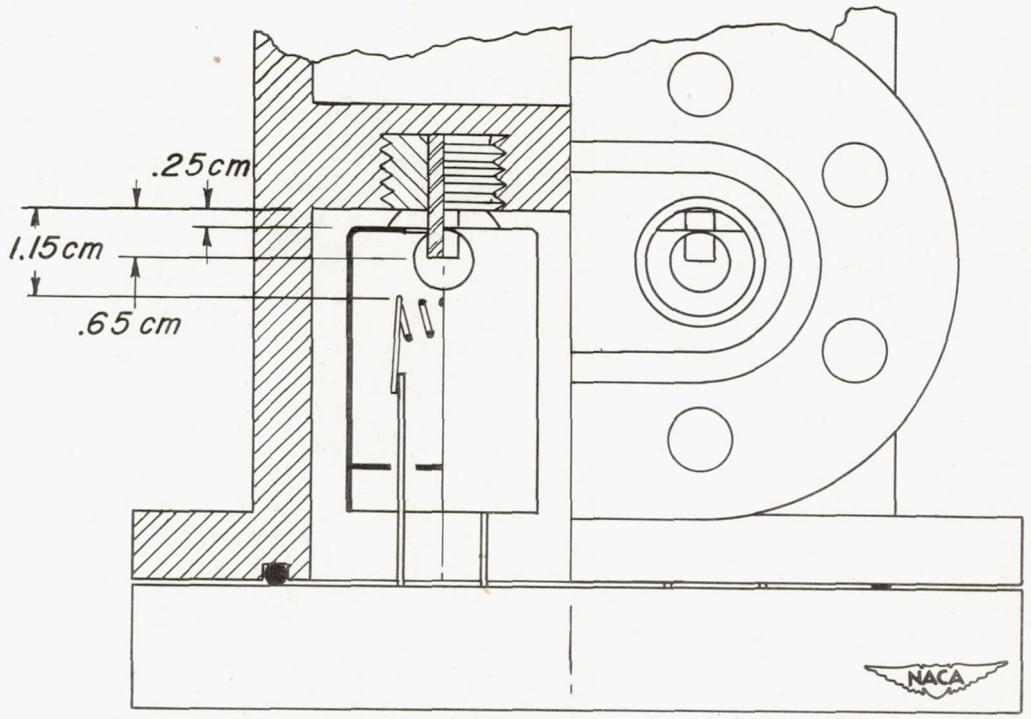

Figure 3.- Cross-sectional drawing, final model of X-ray tube.

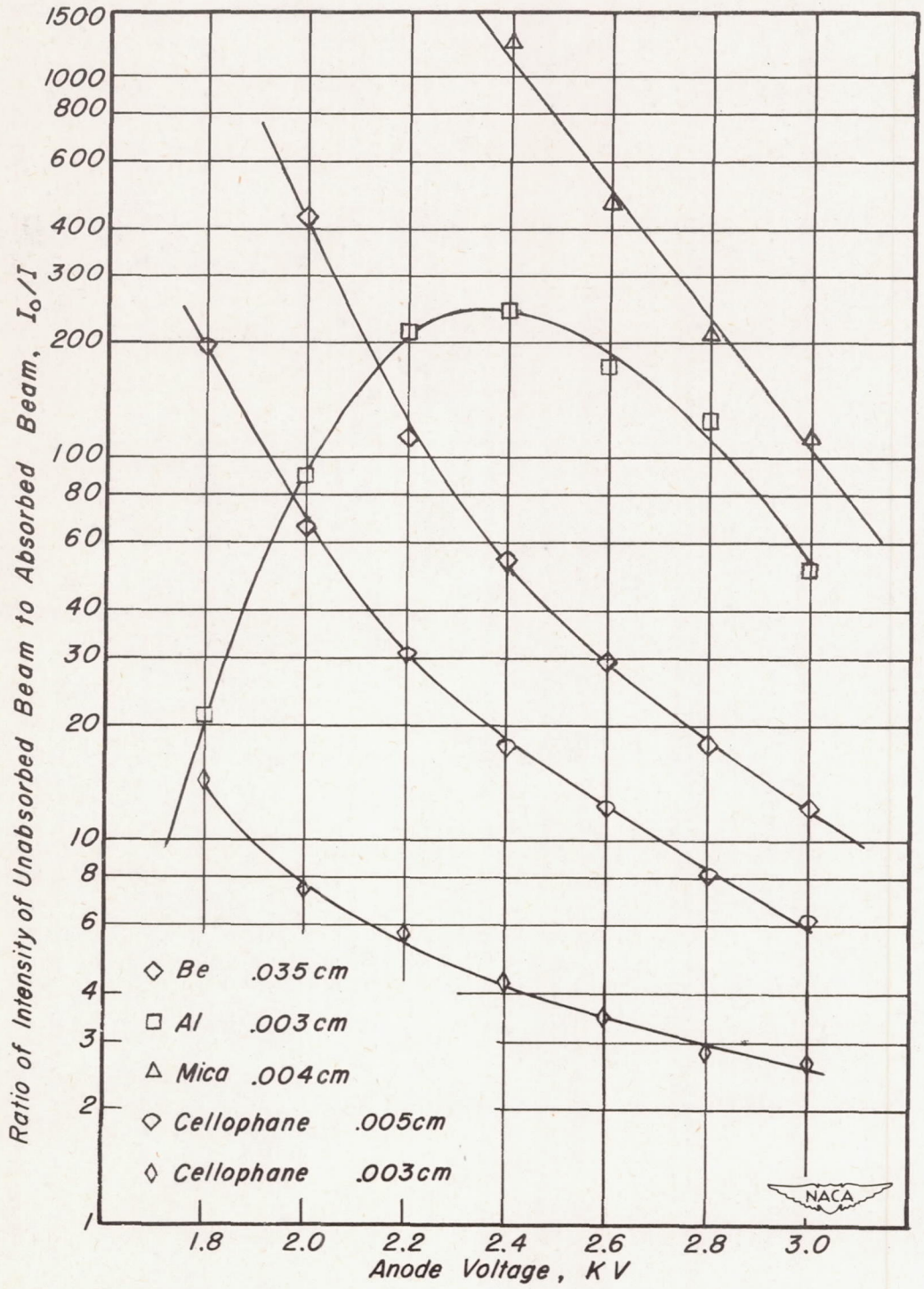

Figure 4.- Absorption losses for a few window materials.

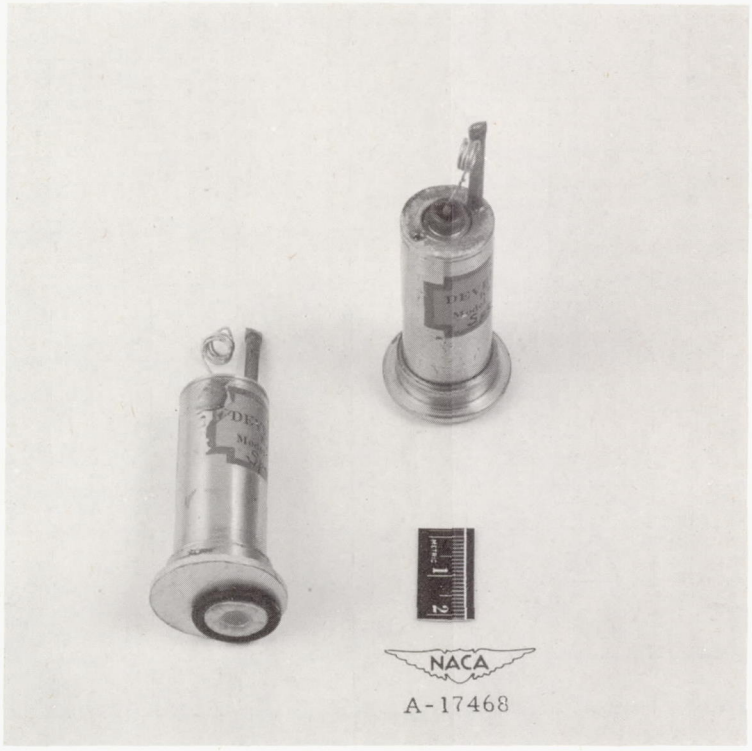

Figure 5.- Geiger-Mueller tube used.

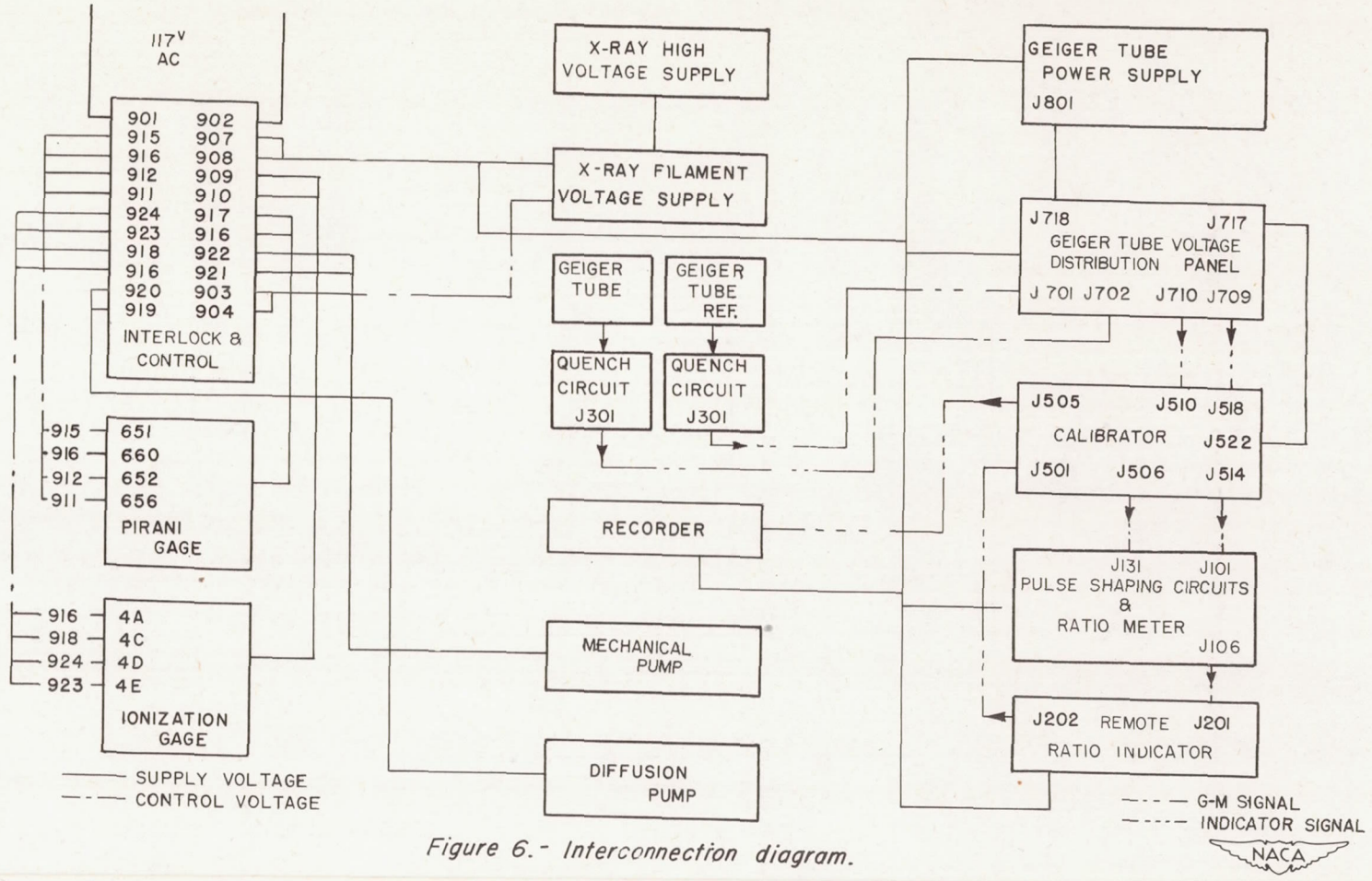

Figure 6.- Interconnection diagram.

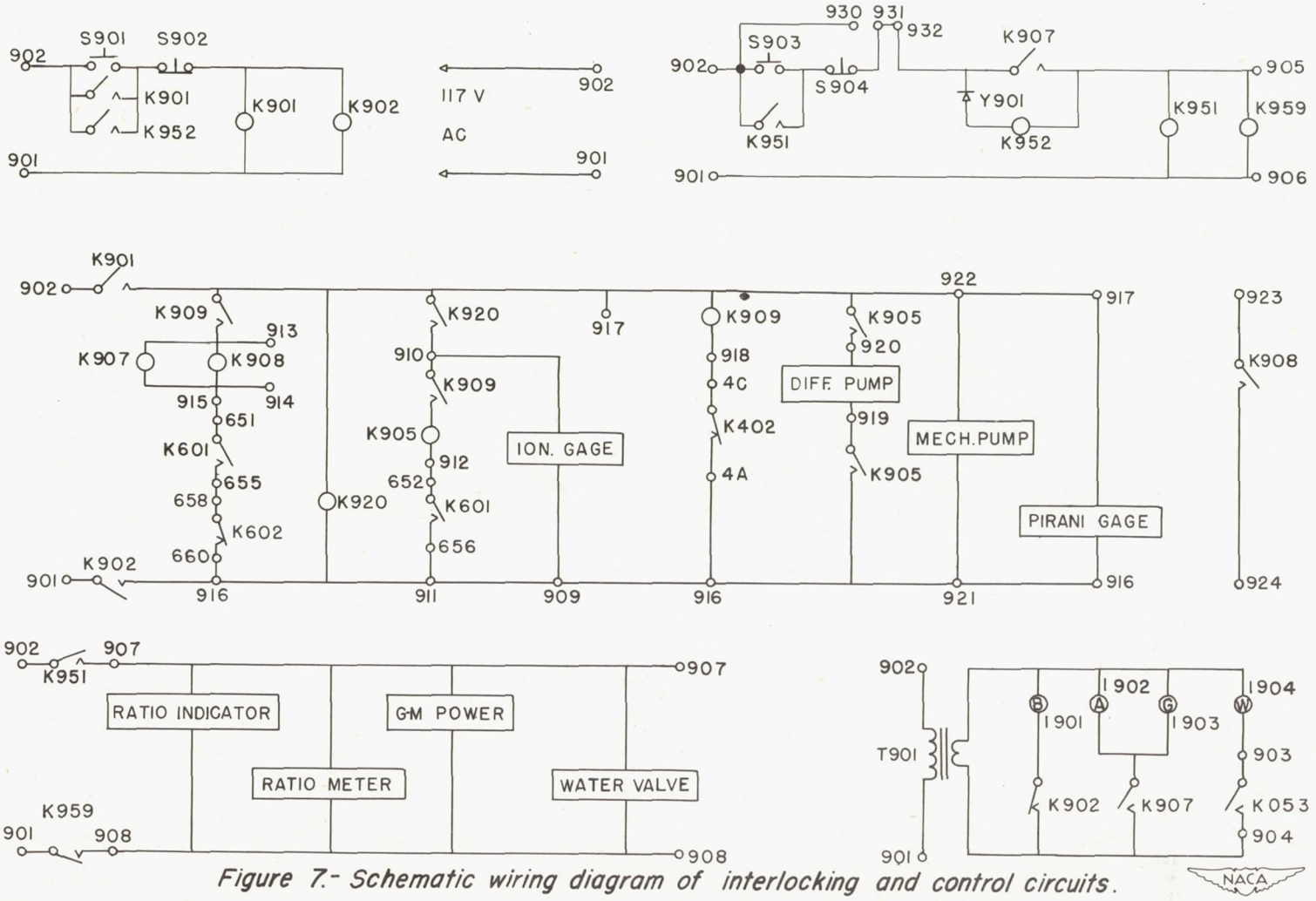

Figure 7.- Schematic wiring diagram of interlocking and control circuits.

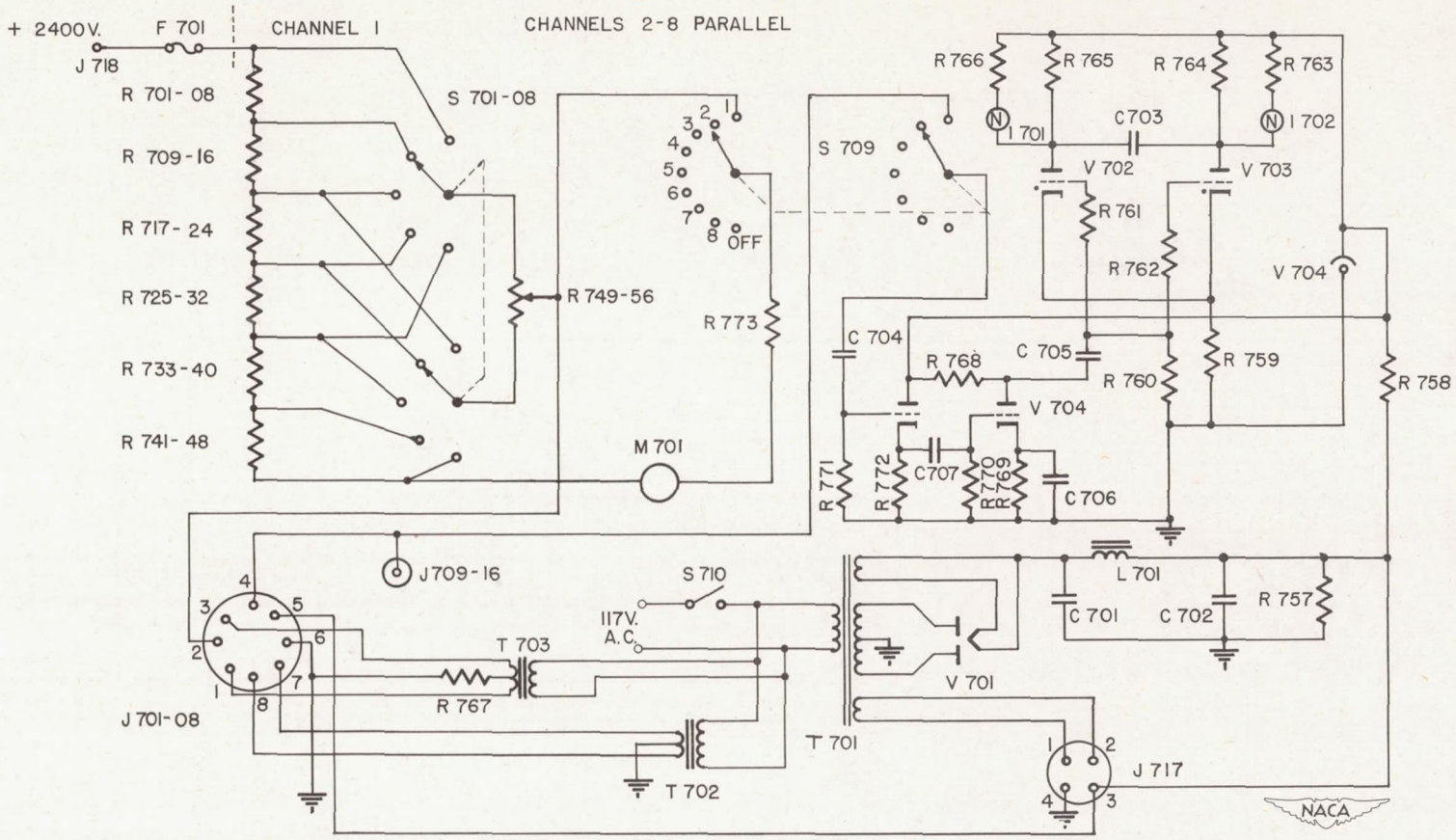

Figure 8.- Schematic diagram of the Geiger Tube voltage distribution panel.

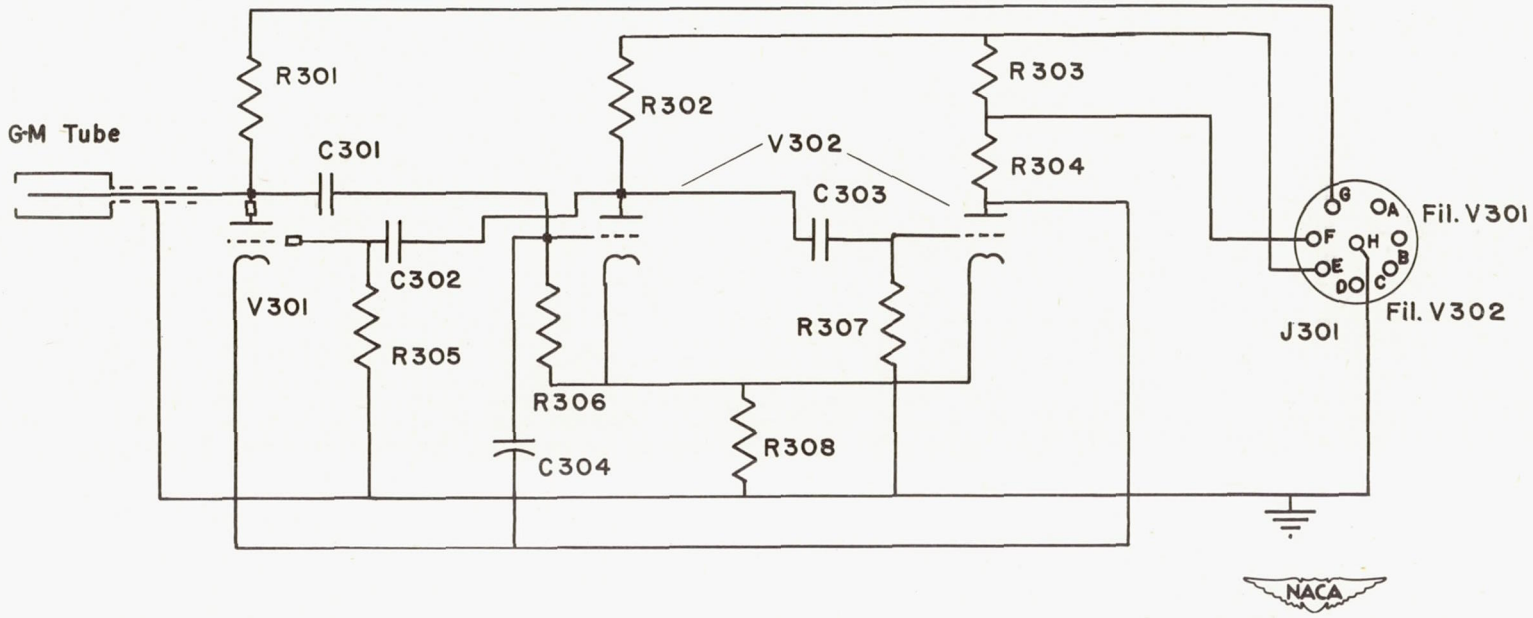

Figure 9.- Schematic wiring diagram of quench circuit.

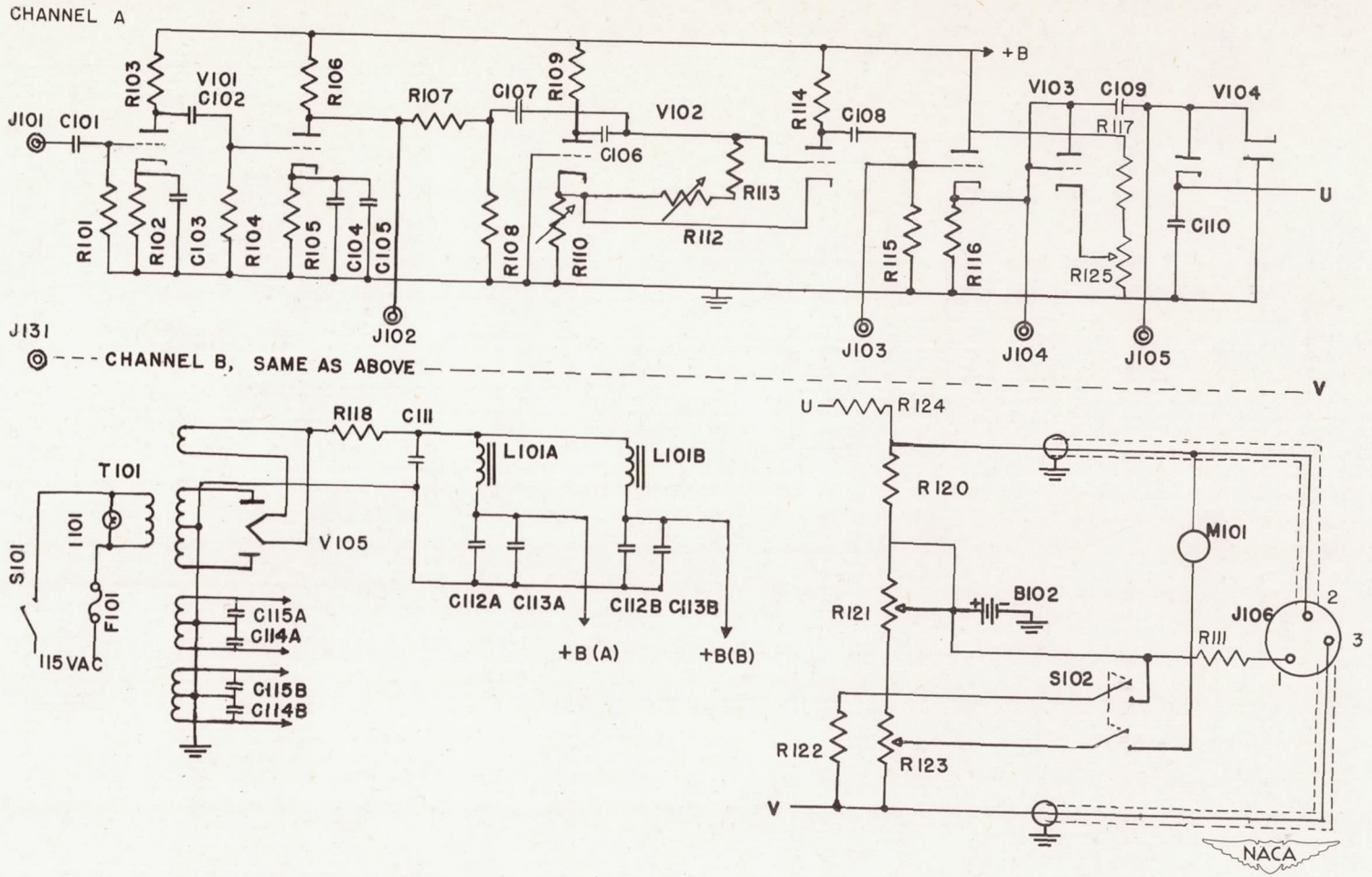

Figure 10.- Schematic wiring diagram of pulse shaping circuits and ratio meter.

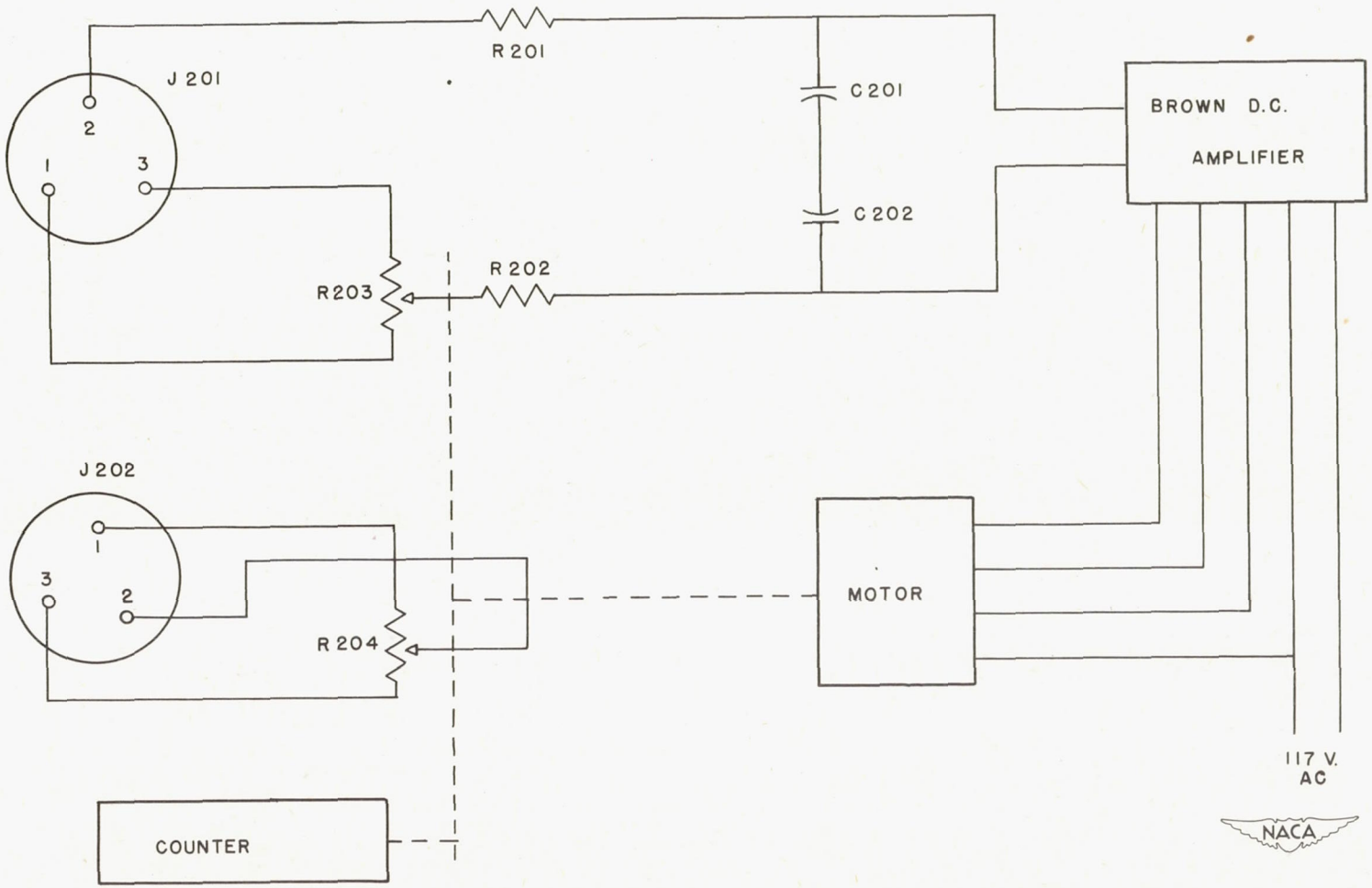

Figure II.- Schematic wiring diagram of remote ratio indicator.

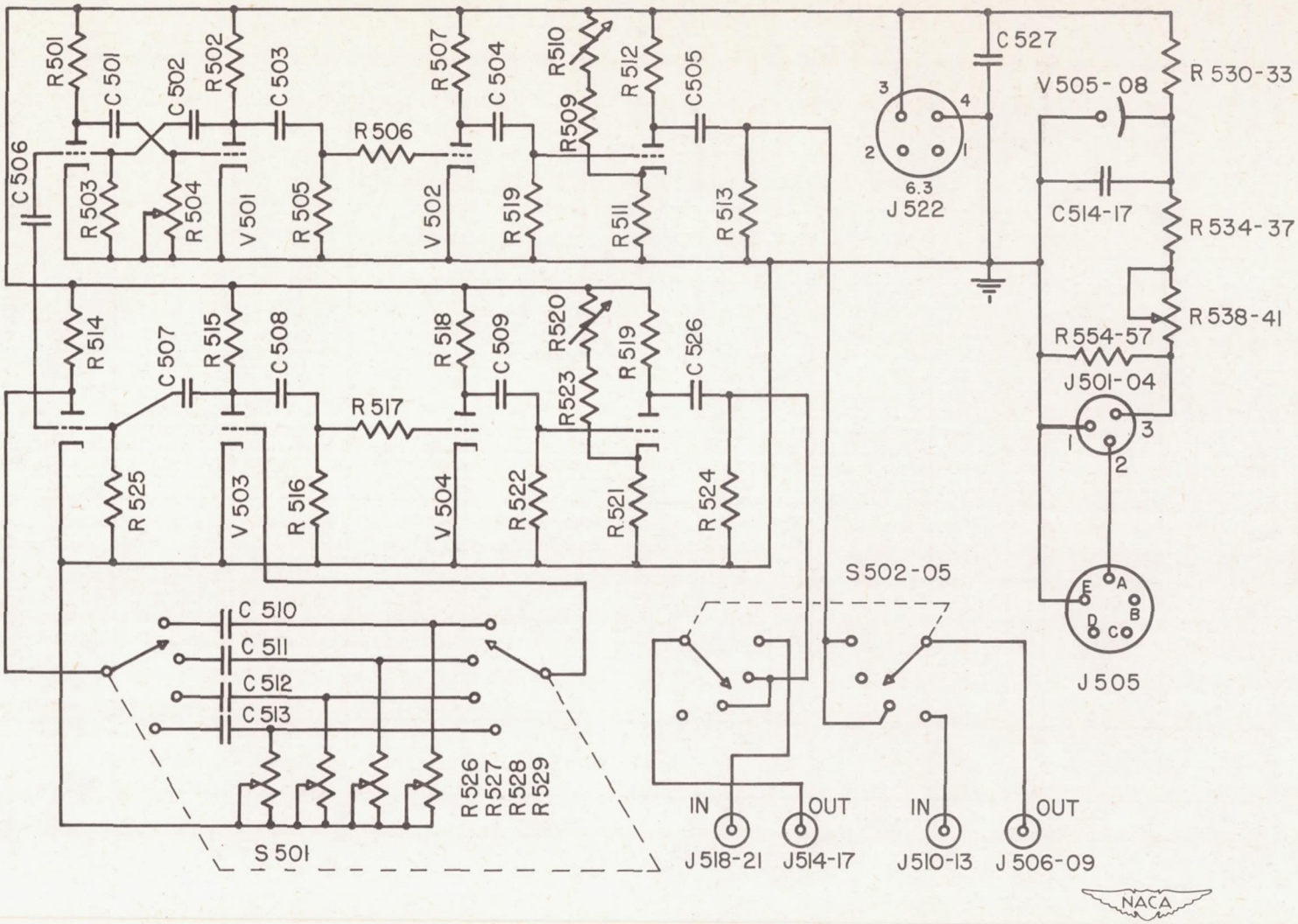

Figure 12.- Schematic wiring diagram of remote-ratio-indicator calibrator

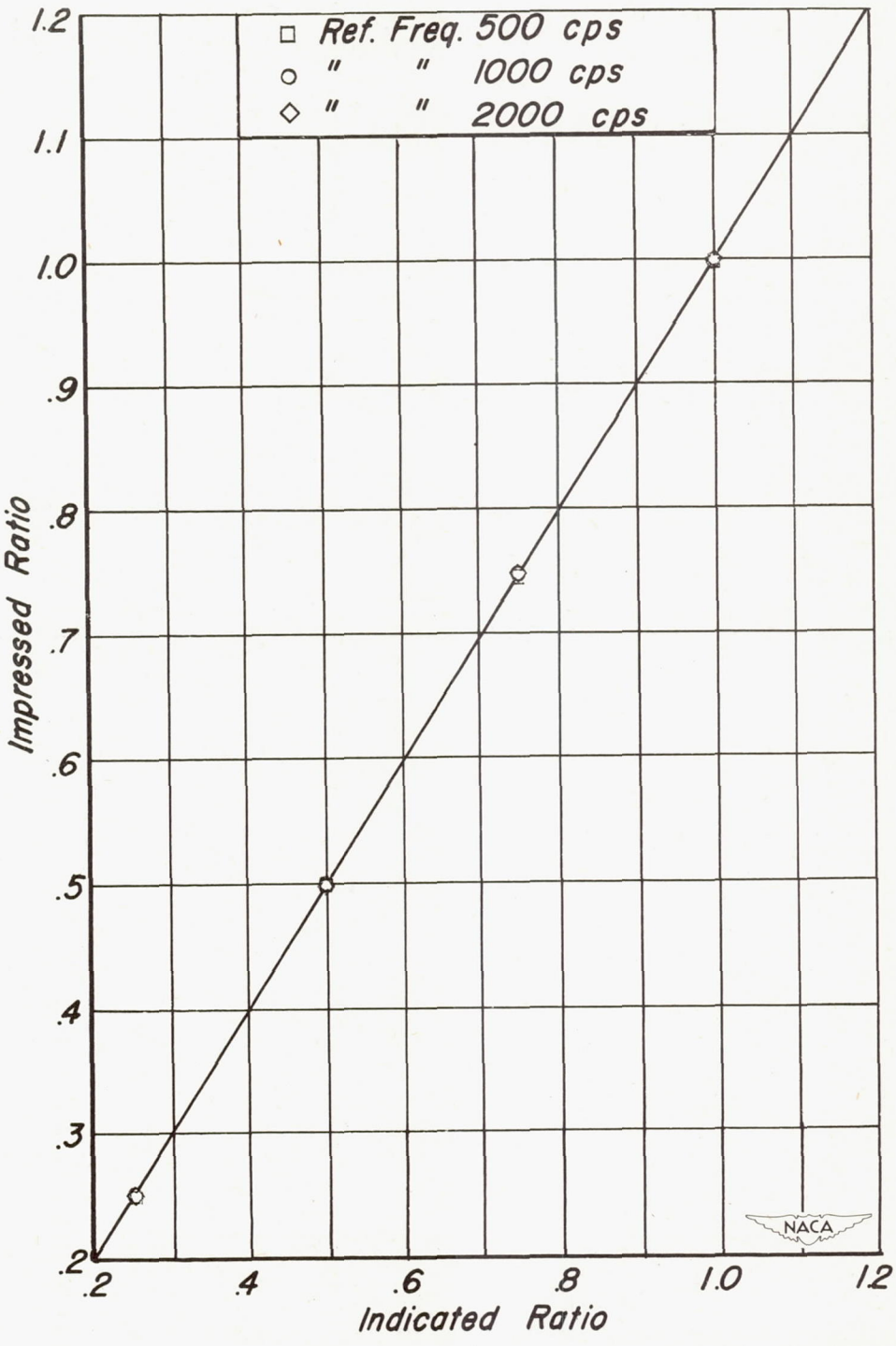

Figure 13.- Ratio given by automatic ratio indicator as a function of impressed ratio.

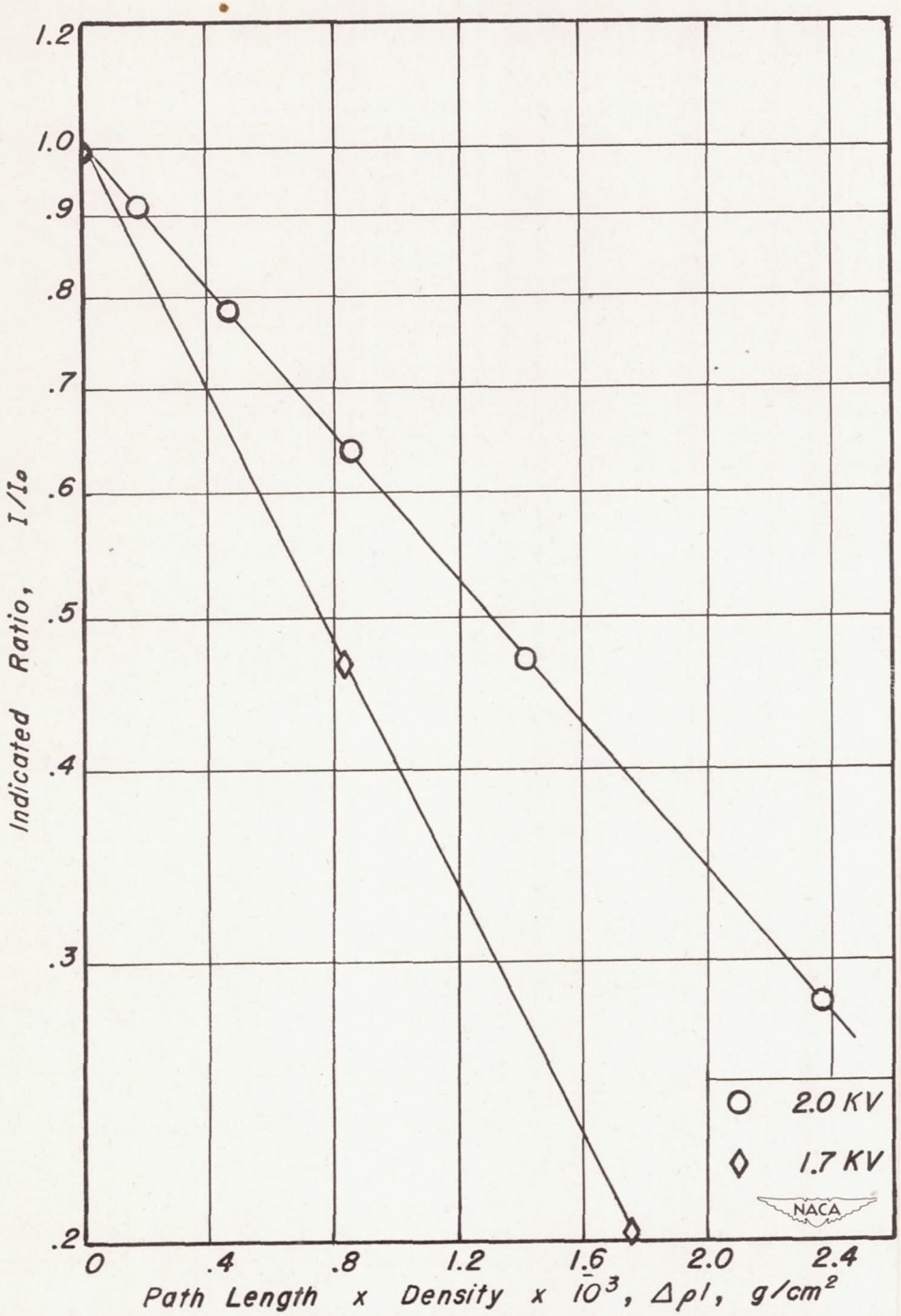

Figure 14.- Typical calibration of densitometer; aperture size 8×10^{-3} cm^2, averaging time 5 minutes.

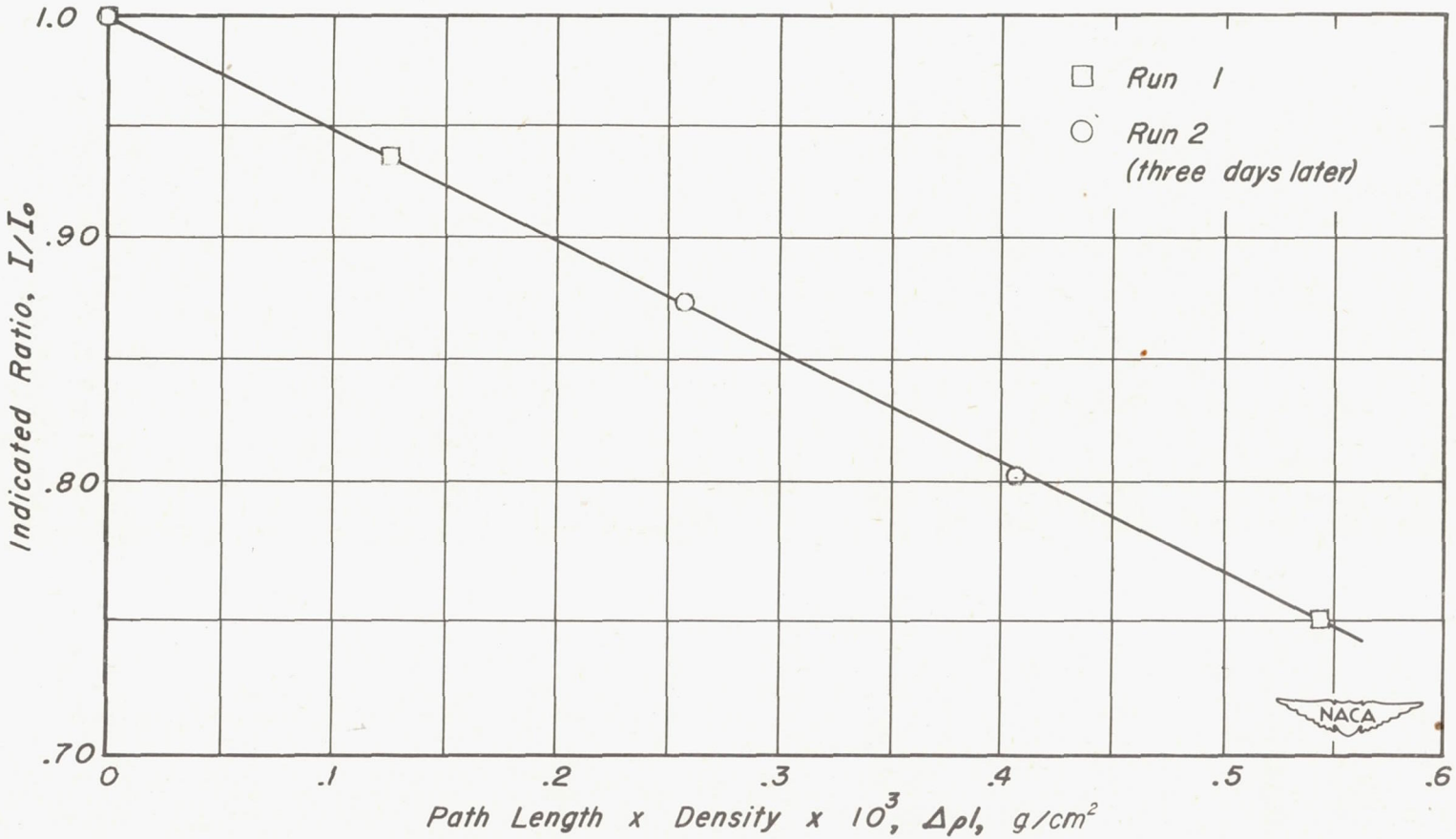

Figure 15.- Repeatability of densitometer; anode voltage of 2KV, aperture size $8 \times 10^{-3} cm^2$, averaging time 5 minutes.

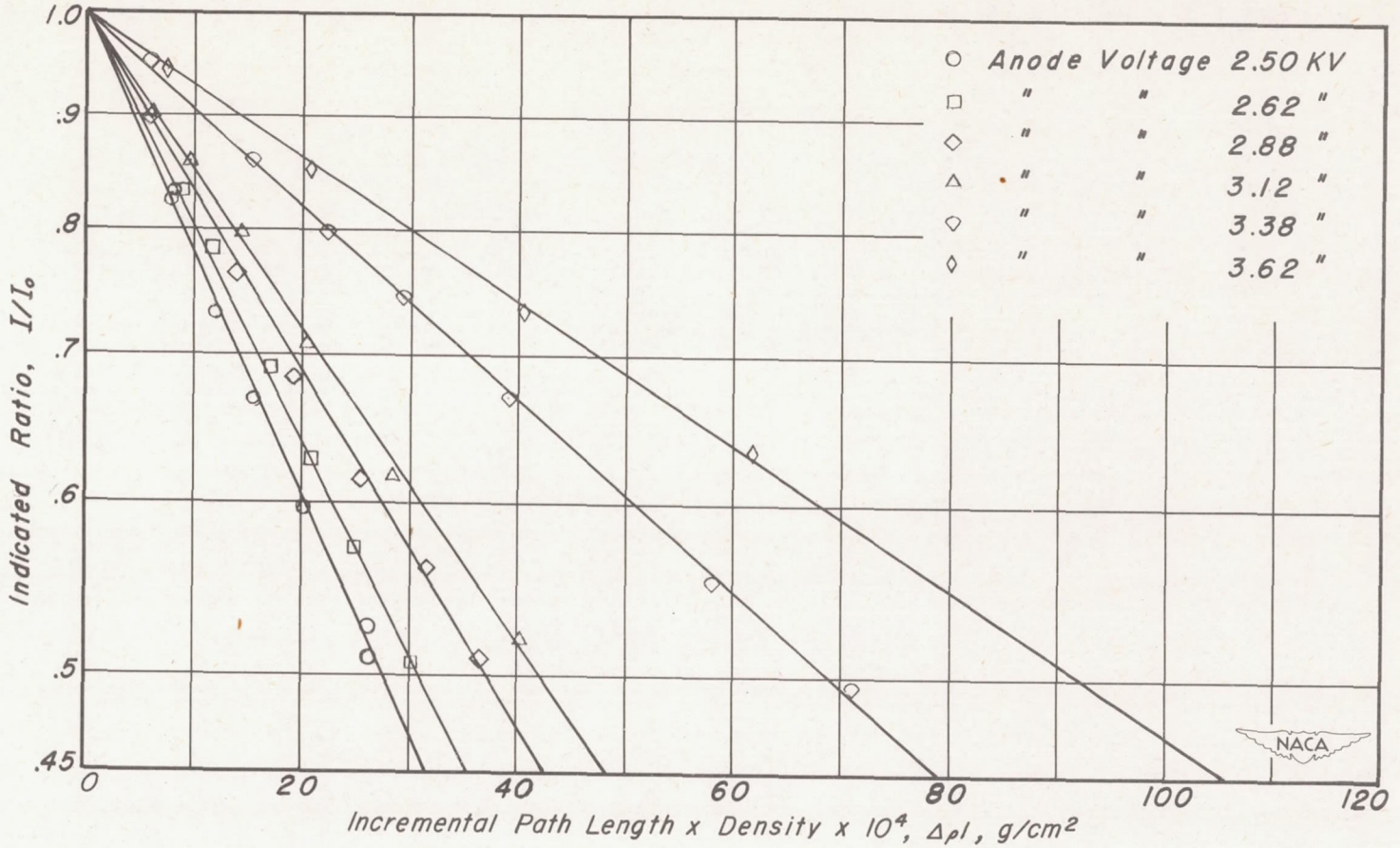

Figure 16.- Typical calibration of densitometer; aperture size 5×10^{-4} cm^2, averaging time 30 seconds.

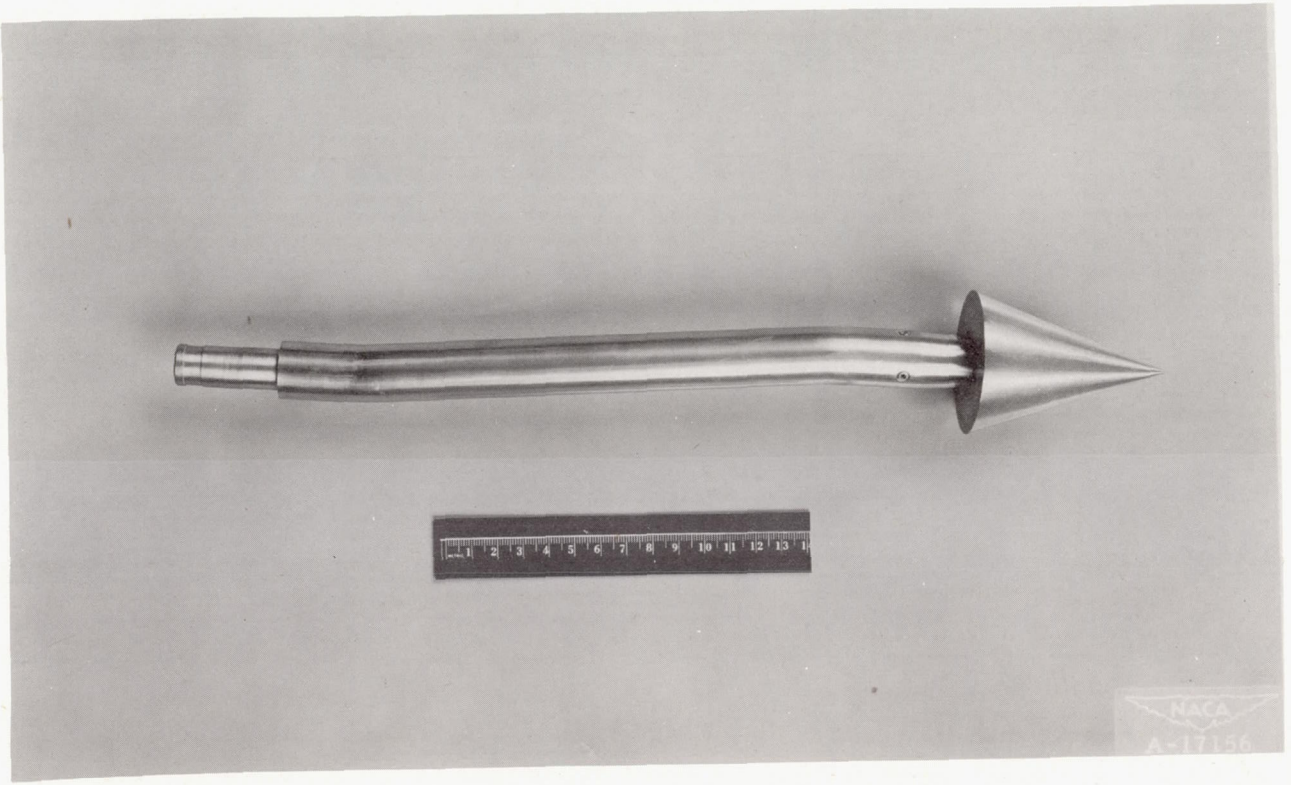

Figure 17.- Model used in tunnel tests shown on offset mounting fixture.

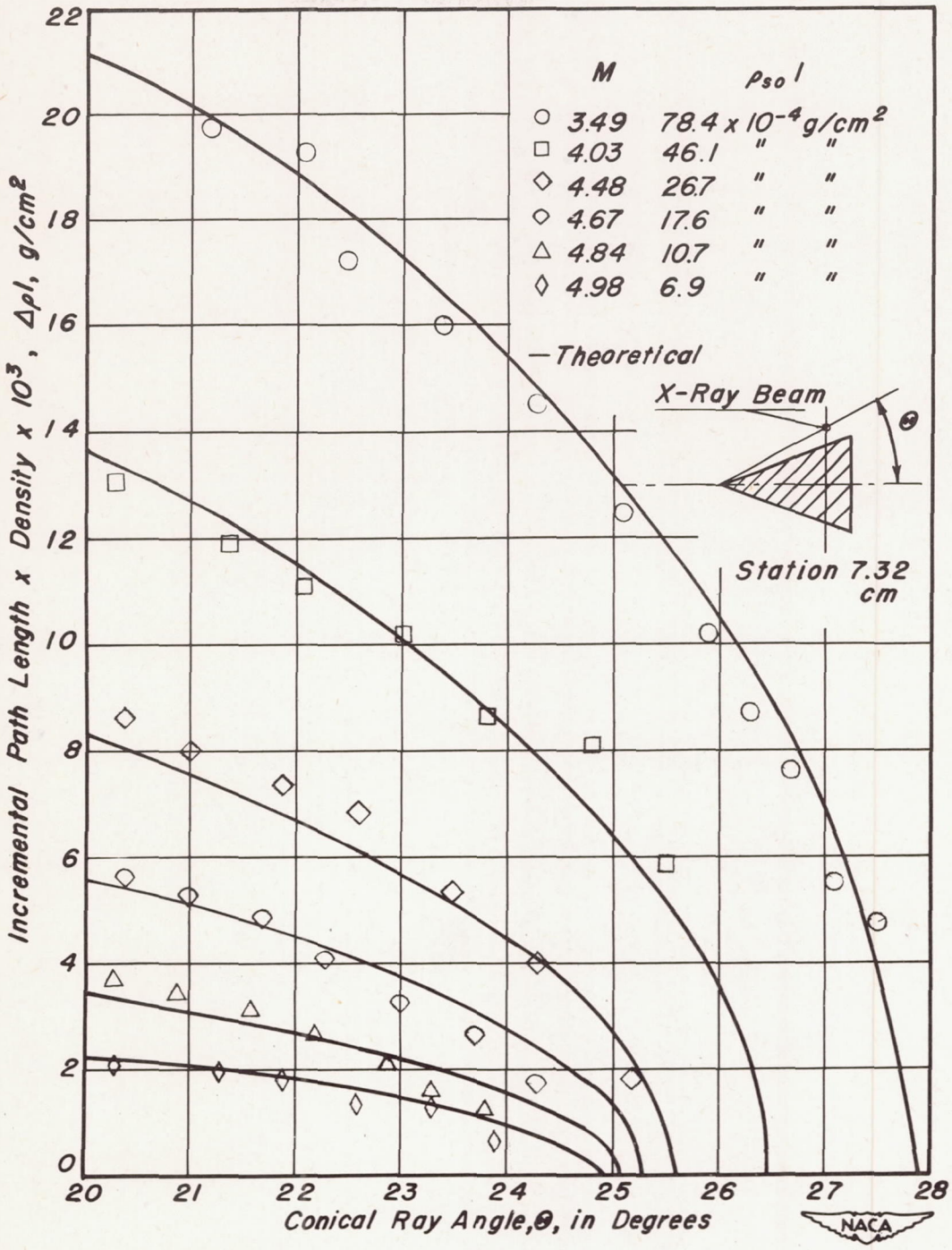

Figure 18.- Increment in density-path-length through the supersonic flow field about 40° cone 7.32 cm downstream of the apex.